Modulation of Core Turbulent Density Fluctuations by Large-Scale Neoclassical Tearing Mode Islands in the DIII-D Tokamak

L. Bardóczi, T. L. Rhodes, T. A. Carter, A. Bañón Navarro, W. A. Peebles, F. Jenko, and G. McKee

Phys. Rev. Lett. **116**, 215001 — Published 26 May 2016

DOI: 10.1103/PhysRevLett.116.215001

Modulation of core turbulent density fluctuations by large-scale Neoclassical Tearing Mode islands in the DIII-D tokamak

L. Bardóczi,[1] T. L. Rhodes,[1] T. A. Carter,[1] A. Bañón Navarro,[1] W. A. Peebles,[1] F. Jenko,[1] and G. McKee[2]

[1] *University of California Los Angeles, Los Angeles, California 90095, USA*
[2] *University of Wisconsin-Madison, Madison, Wisconsin 53706, USA*

(Dated: May 18, 2016)

We report the first observation of localized modulation of turbulent density fluctuations $\widetilde{n}$ (via Beam Emission Spectroscopy) by neoclassical tearing modes (NTMs) in the core of the DIII-D tokamak. NTMs are important as they often lead to severe degradation of plasma confinement and disruptions in high-confinement fusion experiments. Magnetic islands associated with NTMs significantly modify the profiles and turbulence drives. In this experiment $\widetilde{n}$ was found to be modulated by 14% across the island. Gyrokinetic simulations suggest that $\widetilde{n}$ could be dominantly driven by the ion temperature gradient (ITG) instability.

The tearing instability is known to be an important ingredient in astrophysical and laboratory plasmas, e.g. solar flares, coronal mass ejection, the Earth's magnetosphere and magnetically confined fusion plasmas [1]. Neoclassical Tearing Modes (NTMs) form magnetic islands across the nested flux surfaces of tokamaks via magnetic reconnection. NTMs can lead to the degradation of plasma confinement and, if large enough, lead to disruption. The $m/n = 2/1$ NTM is an outstanding, major impediment in the development of operating scenarios in current toroidal fusion devices (m/n is the poloidal/toroidal mode number). Recent theoretical work predicts the reduction of ion temperature gradient driven turbulence (ITG) inside the island resulting from the decreased gradients and turbulence drives at the O-point [2]. Interestingly, despite the increase of gradients just outside the island, turbulence amplitude may not increase substantially due to simultaneous increase in flow shear [3, 4]. It is also predicted that turbulence affects the transport across the island [4] and can diminish the drive of the NTM itself [5]. Non-localized measurements have shown modification of density fluctuations due to tearing instability in TEXT [6]. Recently, it was found in J-TEXT that static magnetic islands induced by resonant magnetic perturbation lead to the decrease of the fluctuation level in the island region [7]. Improved understanding of NTM physics and interaction with turbulence can lead to improved control of NTMs and plasma performance. Therefore, it can have important implications for future fusion devices, in particular for ITER.

In this Letter we report the first experimental observation of significant local reduction of turbulent density fluctuations ($\widetilde{\mathrm{n}}$) at the O-point of a naturally arising, rotating NTM island. These quantitative results on the degree and phasing of the reduction provide the first opportunity for testing of theoretical models and simulations (e.g. recent simulations of self-consistent interaction of NTM and turbulence [8]). This result has potential impact on transport within and growth rate of NTMs.

The fluctuations were measured locally via Beam Emission Spectroscopy (BES) and non-locally via Far Infrared Scattering (FIR). Linear gyrokinetic simulations of these plasmas indicate that these fluctuations are likely due to the ITG instability.

We studied turbulence in the DIII-D tokamak in two H-mode discharges, one with an $m/n = 2/1$ NTM and one without. The relevant plasma parameters are: major radius 1.76 m, minor radius 0.56 m, toroidal magnetic field -1.9 T, plasma current 1 MA, neutral beam power 5 MW (no electron cyclotron heating), line averaged core density $3.4 \times 10^{19}\mathrm{m}^{-3}$ (interferometry [9]), electron temperature 2 keV (Electron Cyclotron Emission [10]) and ion temperature 2.5 keV (Charge Exchange Recombination [11]) at the $q = 2$ rational surface (q is the safety factor). In discharge 134375 a naturally arising, long lived (1 s), quasi-stationary 2/1 NTM island rotates toroidally at about 14.5 kHz as seen from Mirnov-coil measurements. For reference, we compare this plasma with a similar but NTM free discharge (134374). The representative $\mathrm{T_e}$ (electron temperature), $\mathrm{T_i}$ (ion temperature) and $\mathrm{n_e}$ (electron density, Thomson scattering [12]) profiles averaged over 20 ms [Fig. 1 , (b) and (c)] show $\mathrm{T_e}$, $\mathrm{T_i}$ and n reduction in the core, and $\nabla\mathrm{T_e}$, $\nabla\mathrm{T_i}$ and $\nabla\mathrm{n}$ are reduced at $R \approx 200$ cm with NTM (R is the major radius coordinate).

Magnetic islands are identified using the DIII-D ECE radiometer that provides $\mathrm{T_e}$ from measurements of optically thick, second harmonic (X-mode) electron cyclotron emission. $\mathrm{T_e}$ was probed at 40 radial locations with a 480 kHz sampling rate 0.3 cm above the tokamak mid-plane at the $\phi = 81°$ toroidal port. The toroidal rotation of the island and the good access of diagnostics allow the probing of $\mathrm{T_e}$ with respect to the helical phase (ξ) of the island ($\xi = m\theta - n\phi$, where θ and ϕ are the poloidal and toroidal angles). A contour plot of the phase-locked $\mathrm{T_e}$ clearly shows the island centered at $R_\mathrm{s} \approx 199$ cm which is well aligned with the $q = 2$ rational surface [Fig. 1 (d)], as expected from a 2/1 island. The normalized toroidal flux surface label of the $q = 2$ surface is $\rho = 0.38$. The steep X-point ($\xi = 0, 2\pi$) and flattened O-point ($\xi = \pi$) $\mathrm{T_e}$

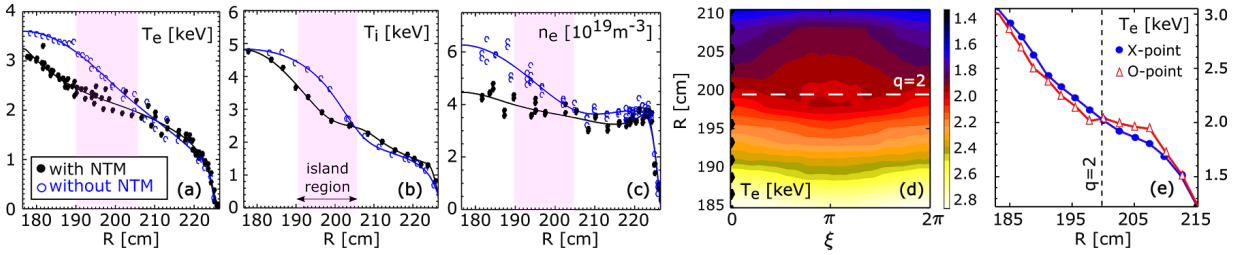

FIG. 1: Representative (a) T_e, (b) T_i and (c) n_e profiles with (134375) and without NTM (134374). (d) Phase-lock averaged T_e contours and (e) T_e profiles across the X-point and O-point of the 2/1 island (134375).

profiles [Fig. 1 (d)] are consistent with an island centered at R_s. The full width of the island is about $W = 15$ cm (defined as the maximum radial distance between the island separatrices), determined by fitting the numerical solutions of the heat transport model of magnetic islands to T_e data by χ^2 minimization [13, 14]. The toroidal Mirnov-coil array data shows a dominant $n = 1$ toroidal harmonic component of magnetic field fluctuations ($\widetilde{B}$) at the tokamak wall which is also consistent with a 2/1 island.

The density fluctuations measured with FIR and BES, respectively, can be mapped to the phase of the island using the T_e measurement as reference. Therefore it is possible to compare X-point and O-point fluctuation levels at frequencies well above the 14.5 kHz NTM frequency to test the response of the broadband turbulence to the island.

The FIR system [15] utilizes an O-mode microwave beam that is scattered by density fluctuations $\widetilde{n}$ along the $\phi = 60°$ chord 7.6 cm above the mid-plane. The scattered radiation is detected near 0° scattering angle which selects $\widetilde{n}(k)$ in the $k_\theta < 1\text{cm}^{-1}$ wavenumber range, where k is the wavenumber of $\widetilde{n}$ in the vertical direction in the lab frame and nearly perpendicular to the magnetic field. At $q = 2$ the ion-gyroradius (ρ_i) is approximately 0.7 cm, so that $k_\theta \rho_i < 0.7$ which is a typical range of the ITG instability. As scattering occurs everywhere along the beam trajectory, the FIR system is a line integral measurement in the mid-plane. The low-k FIR scattering system is then a good monitor of $\widetilde{n}$ along this chord encompassing the radial location and extent of the 2/1 tearing mode. In the following the FIR signal is denoted by $\widetilde{n}|_{\text{FIR}}$.

The BES system [16] detects relative density fluctuations $\widetilde{n}/n|_{\text{BES}}$ locally by measuring the light emission from the neutral beam at $\phi = 150°$, 3.6 cm above the mid-plane in the major radius range of about R=180-230 cm which covers the 2/1 island region. The BES system is sensitive to localized, long-wavelength density fluctuations of $k_\theta < 1$ cm^{-1} corresponding to the ITG wavenumber range ($k_\theta \rho_i < 0.7$) similarly to the FIR system. The typical separation between the analyzed 26 channels is about 1 cm, the radial and poloidal localization is about 1 cm.

The relative fluctuation levels $\widetilde{n}/n|_{\text{BES}}$ measured at R_s in the two discharges at R_s are the same, but the absolute fluctuation levels are about $5 \cdot 10^{17}$ m^{-3} without NTM and $4 \cdot 10^{17}$ m^{-3} with NTM; i.e., broadband fluctuations are smaller with NTM, consistent with the T_e, T_i and n_e gradients [Fig. 1 (a), (b) and (c)].

The island rotates with 14.5 kHz as seen from the spectrum of $\widetilde{B}$ [Fig. 2 (a)]. Similarly to T_e, it is expected that n is also flattened at the O-point [17], hence n measured in the lab-frame is expected to be modulated due the island rotation. This 14.5 kHz modulation is seen in the spectrum of $\widetilde{n}|_{\text{FIR}}$ [Fig. 2 (b)] and $\widetilde{n}/n|_{\text{BES}}$ [Fig. 2 (c)] measured 0.3 cm inside R_s. For reference, we compare with $\widetilde{n}|_{\text{FIR}}$ measured before NTM onset and with $\widetilde{n}/n|_{\text{BES}}$ measured during the same window (with NTM) but further out where the effect of the island is not dominant ($\rho \approx 0.75$, 17 cm away from R_s).

Before NTM onset there is no coherent peak at 14.5 kHz in the spectrum of the reference $\widetilde{B}$ and $\widetilde{n}|_{\text{FIR}}$ [Fig. 2 (a) and (b)] and the spectrum of the reference $\widetilde{n}/n|_{\text{BES}}$ shows no coherent modulation either [Fig. 2 (c)]. Hence the peak at 14.5 kHz seen in the $\widetilde{n}|_{\text{FIR}}$ and $\widetilde{n}/n|_{\text{BES}}$ spectra is identified as the local density profile modulation due to the island rotation. Cross-correlation analysis of $\widetilde{n}|_{\text{FIR}}$ with $\widetilde{B}$ and $\widetilde{n}/n|_{\text{BES}}$ with $\widetilde{B}$ confirms this point.

Besides the coherent peak at 14.5 kHz (and higher harmonics) the $\widetilde{n}|_{\text{FIR}}$ and $\widetilde{n}/n|_{\text{BES}}$ signals possess broadband fluctuations up to about 500 kHz attributed to the effect of broadband turbulent density fluctuations [Fig. 2 (b) and (c)]. Next we look at the modulation of turbulence by analyzing the envelope of the fluctuations in the $\Delta f = 100 - 500$ kHz range (shaded in Fig. 2 (b) and (c)). The envelope $\Psi^{\text{FIR}}_{\widetilde{n}}(t)$ of $\widetilde{n}(t)|_{\text{FIR}}$ is calculated as:

$$\Psi^{\text{FIR}}_{\widetilde{n}}(t) = \left(\int_{100\ \text{kHz}}^{500\ \text{kHz}} \widetilde{n}(f)|_{\text{FIR}} \cdot e^{i2\pi f t} df \right)^2 \qquad (1)$$

where f is the frequency and $\widetilde{n}(f)|_{\text{FIR}}$ is the Fourier transform of $\widetilde{n}(t)|_{\text{FIR}}$. The envelope of $\widetilde{n}(t)/n(t)|_{\text{BES}}$ and $\widetilde{B}(t)$ are calculated similarly and denoted as $\Psi^{\text{BES}}_{\widetilde{n}/n}(t)$ and $\Psi_{\widetilde{B}}(t)$, respectively, while the Fourier transforms are $\Psi^{\text{FIR}}_{\widetilde{n}}(f)$, $\Psi^{\text{BES}}_{\widetilde{n}/n}(f)$ and $\Psi_{\widetilde{B}}(f)$, respectively. $\Psi_{\widetilde{B}}(f)$ has no coherent peak at 14.5 kHz, hence the measured

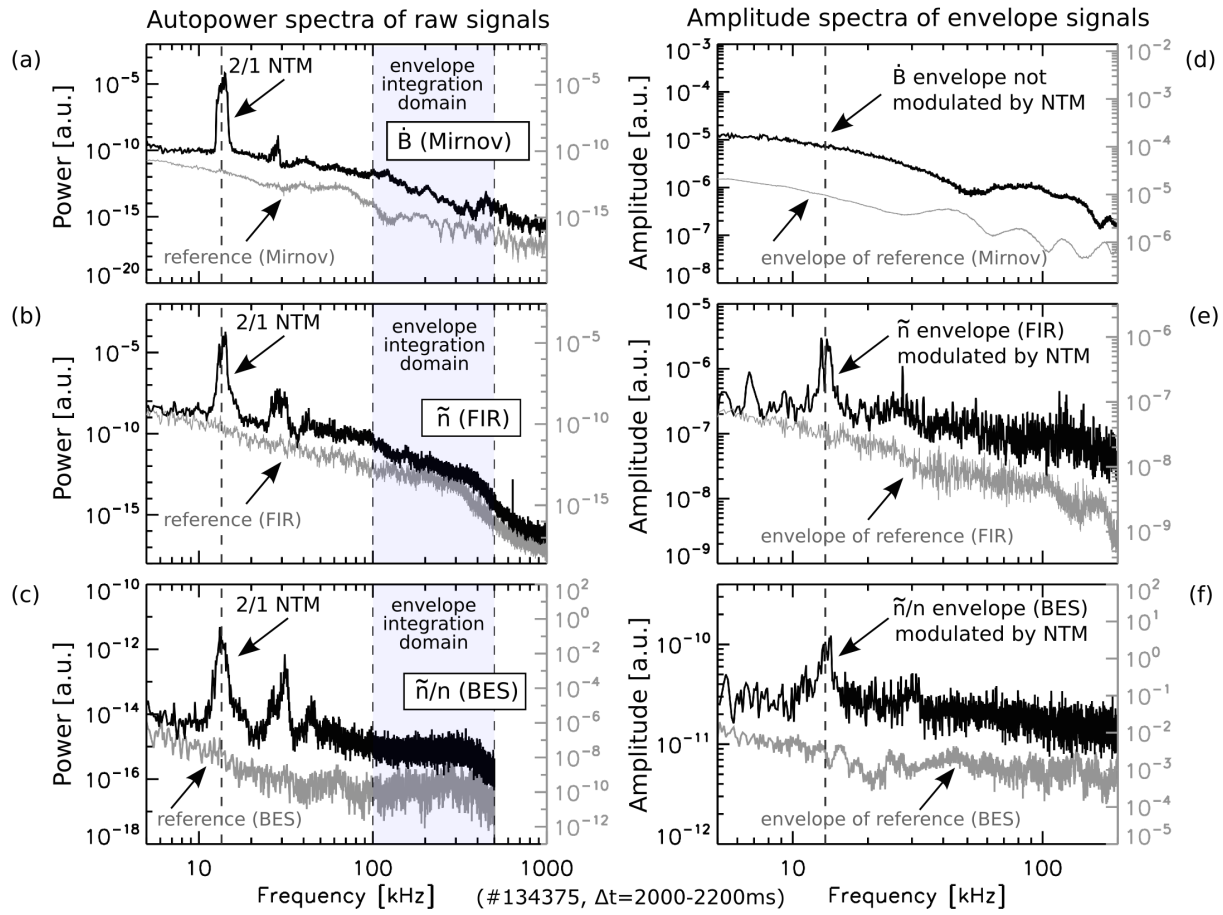

FIG. 2: Power spectrum of (a) $\widetilde{\mathrm{B}}$ (Mirnov), (b) $\tilde{\mathrm{n}}|_{\mathrm{FIR}}$ and (c) $\tilde{\mathrm{n}}/\mathrm{n}|_{\mathrm{BES}}$. Amplitude spectrum of the corresponding envelope signals: (d) envelope of $\widetilde{\mathrm{B}}$, (e) envelope of $\tilde{\mathrm{n}}|_{\mathrm{FIR}}$ and (f) envelope of $\tilde{\mathrm{n}}/\mathrm{n}|_{\mathrm{BES}}$. Note that the magnetic and FIR reference signals (light color) were measured before NTM onset, while the reference BES signal was measured during NTM but further out (17 cm away from R_{s} showing the radial and temporal localization of the NTM.

broadband $\widetilde{\mathrm{B}}(t)$ is not modulated by the rotating island [Fig. 2 (d)]. This is consistent with expectation as the magnetic field B_θ of a poloidal harmonic component of the perturbed current located at r_{s} decays as $\mathrm{B}_\theta(\mathrm{b}_\circ) \propto (r_{\mathrm{s}}/\mathrm{b}_\circ)^{m+1}$, where $\mathrm{b}_\circ$ is the probing location. Therefore the measured broadband magnetic fluctuations originate from the edge plasma, not from the island region.

$\Psi^{\mathrm{FIR}}_{\tilde{\mathrm{n}}}(f)$ and $\Psi^{\mathrm{BES}}_{\tilde{\mathrm{n}}/\mathrm{n}}(f)$ [Fig. 2 (e) and (f)] exhibit a clear peak at the NTM frequency (and additionally at the second harmonic frequency) showing the modulation of broadband turbulence across the island. The envelopes of the reference signals show no turbulence modulation (without island), as expected [Fig. 2 (e) and (f)].

Both the FIR and BES systems detect the reduction/increase of the broadband turbulent density fluctuations at the O-point/X-point region of the island. As the diagnostics are separated toroidally and poloidally, they probe different phases of the island at a given instant of time. Due to the island rotation this offset translates to an effective time lag: $\Delta t = \Delta\xi/\omega$, where $\Delta\xi = -n(\Delta\phi - 2\pi\iota^{-1}\Delta\theta)$, ω is the NTM frequency and ι is the rotational transform. Given the probing locations the helical phase differences are $\Delta\xi|_{\mathrm{FIR}} = -12^\circ$ and $\Delta\xi|_{\mathrm{BES}} = -84^\circ$, the time lags are $\Delta t|_{\mathrm{FIR}} = 2.3\ \mu$s and $\Delta t|_{\mathrm{BES}} = 1.6\ \mu s$ relative to the $\mathrm{T_e}$ measurement.

$\Psi^{\mathrm{FIR}}_{\tilde{\mathrm{n}}}(t)$ and $\Psi^{\mathrm{BES}}_{\tilde{\mathrm{n}}/\mathrm{n}}(t)$ were shifted by $\Delta t|_{\mathrm{FIR}}$ and $\Delta t|_{\mathrm{BES}}$, respectively, and bandpass filtered to $\Delta f = 10 - 50$ kHz. These signals are shown in Fig. 3 together with $\mathrm{T_e}$ inside ($R_{\mathrm{s}} > R = 194.7$ cm) and outside ($R_{\mathrm{s}} < R = 204.3$ cm) the $q = 2$ surface. The minima/maxima of $\Psi^{\mathrm{FIR}}_{\tilde{\mathrm{n}}}(t)$ and $\Psi^{\mathrm{BES}}_{\tilde{\mathrm{n}}/\mathrm{n}}(t)$ are close to the minima/maxima of $\mathrm{T_e}(R < R_{\mathrm{s}})$ which correspond to the O-point/X-point passing-by-times. The measured phase lags are $\Delta\xi|_{\mathrm{FIR}} = -12.06^\circ$ (0.5% difference from the estimated -12°) with $\gamma \approx 0.5$ coherence (0.14 significance level) and $\Delta\xi|_{\mathrm{BES}} = -90^\circ$ (6% difference from the estimated -84°) with $\gamma \approx 0.67$ coherence at 14.5 kHz (0.22 significance level). Here $\Psi^{\mathrm{BES}}_{\tilde{\mathrm{n}}/\mathrm{n}}(t)$ was calculated using the nearest neighbor cross-powers, which removes any spuri-

ous contributions of photon noise modulation present in the BES signal. As the BES channels are separated radially by about $1.25\rho_i$, the photon noise is uncorrelated between neighboring channels but the turbulence is correlated.

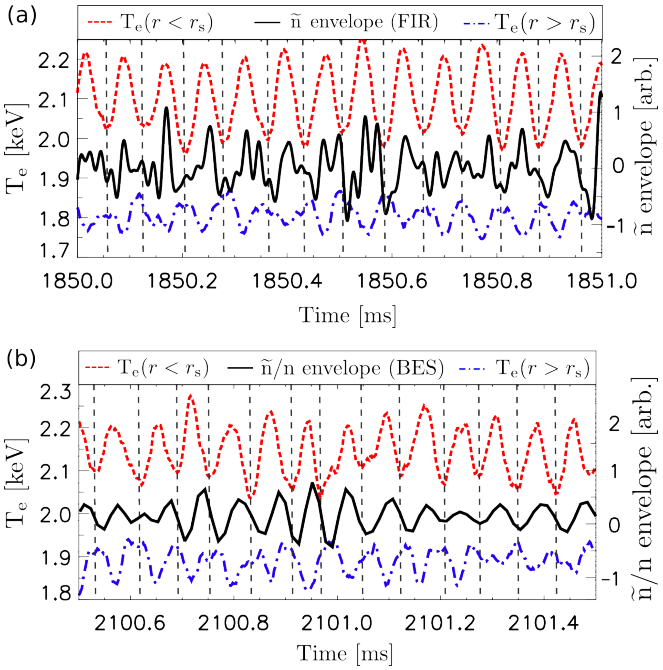

FIG. 3: T_e outside ($R_s < R = 204.3$ cm) and inside ($R_s > R = 194.7$ cm) $q = 2$ and the envelope of (a) $\tilde{n}|_{FIR}$ and (b) $\tilde{n}/n|_{BES}$. O-point passing-by-times are marked by vertical dashed lines (134375).

Small differences between the calculated and measured phases can be explained as r_s changes over time by about 2 cm (8%) resulting in a small change in $\Delta\theta$. Another, also small contribution comes from the phase asymmetry of the island [18]: the typical phase difference between two T_e signals measured on the same side of the island is $\leq 4°$.

Turbulence is modulated by a maximum between 13-14% and this modulation is confined to the island region [Fig. 4 (a)] (the island region is determined by the maximum radial distance between the island separatrices as mentioned previously).

The modulation has near constant phase across the island region. This is consistent with gradient driven turbulent fluctuations being modulated by the rotating island since ∇T_e, ∇T_i and ∇n exhibit no phase jump at R_s. Fig. 4 (b) shows that the relative phase between turbulence modulation and $T_e(R < R_s)$ is nearly constant and near zero across the island. As $T_e(R < R_s)$ has minima at the O-point region the near zero phase means that turbulent fluctuations are smaller at the O-point region ($\tilde{n} \approx 3.6 \times 10^{17}$ m^{-3}) and larger at the X-point region ($\tilde{n} \approx 4.4 \times 10^{17}$ m^{-3}), i.e the modulation shown in Fig. 4 (a) is in fact a reduction of the O-point $\tilde{n}/n|_{BES}$ below the X-point $\tilde{n}/n|_{BES}$.

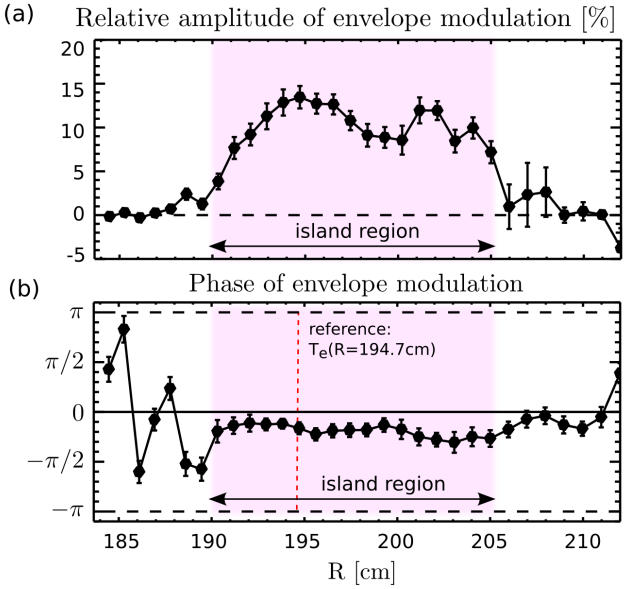

FIG. 4: (a) Modulation amplitude of broadband turbulence relative to the mean fluctuation levels (BES) and (b) phase of modulation relative to $T_e(R < R_s)$ (134375).

It is of interest to better understand the instability or instabilities responsible for the measured fluctuations (e.g. type of instability, drive and damping mechanisms). As a simplified first cut at this we utilized linear GENE gyro-kinetic simulations [19]. These flux-tube simulations focused on ion-scales ($k_\theta \rho_i = 0.1 - 1.0$) and used two fully kinetic species (deuterons and electrons) and included electromagnetic effects. The input experimental profiles (T_e, T_i and n_e [Fig. 1 (a), (b) and (c), respectively]) were averaged over 20 ms (300 island cycles) due to diagnostic limitation hence the simulation predicts the growth rate of the fastest growing micro-instability of the background plasma. As such, the results only give a general idea of the type of micro-instability that could be responsible for the measured fluctuations in the experiment. More complete simulations (such as [8]) are required to fully investigate the turbulence in the presence of islands.

Fig. 5 depicts the growth rates and the frequencies at $q = 2$ versus the wavenumber of ion temperature gradient (ITG) modes, which are identified in GENE by a positive sign of the drift frequency (indicating an ion diamagnetic drift) and their sensitivity with respect to the ion logarithmic temperature gradient ($\Omega_i = -T_i^{-1} \partial T_i / \partial \rho$).

In summary, we showed that 2/1 islands modify/interact with broadband turbulence in the island region. The FIR and BES systems detect the reduction of the broadband turbulent fluctuations in sync with the O-point of the island. The difference between the O-point and X-point turbulence fluctuation levels is about 26%

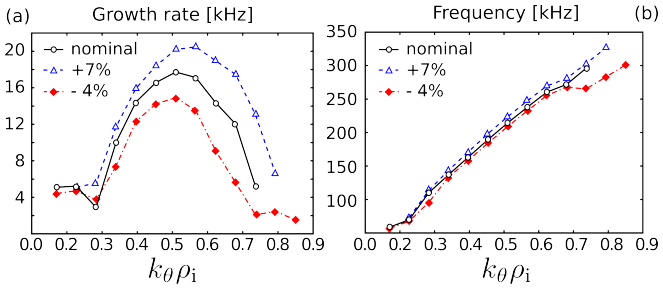

FIG. 5: (a) Linear growth rates and (b) frequencies of the fastest growing micro-instability. $+7\%/-4\%$ change of Ω_i results in $\pm 15\%$ change of the growth rate.

compared to the mean fluctuation levels. This modulation has near constant phase across the island which is consistent with gradient driven fluctuations being modulated by the rotating island. Our local measurements do not show increased turbulence just outside the island where the gradients are elevated (i.e. the envelope is not modulated outside the island region [Fig. 4 (a)]), possibly due to shear flow stabilization as predicted by theory [3, 4].

Local flux-tube simulations using GENE suggest that the ITG instability could be responsible for the observed fluctuations. This possibility is consistent with the wavenumber sensitivity of the BES and FIR diagnostics. Our measurements of reduced fluctuation amplitudes at the O-point of NTM islands are consistent with theoretical predictions for the ITG instability [2, 4].

The observed decrease of $\widetilde{n}$ at the O-point region suggests an explanation for the reduced cross-field thermal diffusivity ($\chi_\perp$) reported in [13]. This is important as the reduction of $\chi_\perp$ is suspected to have a destabilizing role in the NTM dynamics (within the framework of the modified Rutherford equation [20]) via resulting changes in profiles and bootstrap current.

This work was supported in part by the U.S. Department of Energy under DE-FG02-08ER54984, DE-FG03-86ER53266 and DE-FC02-04ER54698. The gyrokinetic simulations presented in this work used resources of the National Energy Research Scientific Computing Center, a DOE Office of Science User Facility supported by the Office of Science of the U.S. Department of Energy under Contract No. DE-AC02-05CH11231.

[1] Masaaki Yamada, et al. *Rev. Mod. Phys.*, 82(603), 2010.
[2] H. R. Wilson et al. *Plasma Phys. Control. Fusion*, 51(115007), 2009.
[3] E. Poli, et al. *Nucl. Fusion*, 49(075010), 2009.
[4] W. A. Hornsby, et al. *Phys. Plasmas*, 17(092301), 2010.
[5] W A Hornsby, et al. *Plasma Phys. Control. Fusion*, 53(054008), 2011.
[6] Changxuan YU, et al. *Nucl. Fusion*, 32(9), 1992.
[7] K.J. Zhao, et al. *Nucl. Fusion*, 55(073022), 2015.
[8] W. A. Hornsby, et al. *Plasma Phys. Control. Fusion*, 57(054018), 2015.
[9] M. A. Van Zeeland, et al. *Rev. Sci. Instrum*, 77(10F325), 2006.
[10] M. E. Austin et al. *Rev. Sci. Instrum.*, 74:1457, 2003.
[11] K. H. Burrell, et al. *Rev. Sci. Instrum*, 75(10), 2004.
[12] T. N. Carlstrom, et al. *Rev. Sci. Instrum*, 63(10):4901–4906, 1992.
[13] L Bardoczi, et al. *accepted in PoP*, 2016.
[14] J. A. Snape, et al. *Plasma Phys. Control. Fusion*, 54(085001), 2012.
[15] T. L. Rhodes, et al. *Rev. Sci. Instrum.*, 77(10E922), 2006.
[16] G. McKee, et al. *Rev. Sci. Instrum.*, 70(913), 1999.
[17] R. Fitzpatrick. *Physics of Plasmas*, 2:825, 1994.
[18] D De Lazarri et al. *Plasma Phys. Control. Fusion*, 53(035020), 2011.
[19] F. Jenko, et al. *Phys. Plasmas*, 7(1904), 2000.
[20] R. Carrera, et al. *Phys. Fluids*, 29(899), 1986.